

Deformation of extreme viscoelastic metals and composites

Y.C. Wang, M. Ludwigson, R.S. Lakes*

Department of Engineering Physics, Engineering Mechanics Program, University of Wisconsin-Madison,
147 ERB, 1500 Engineering Drive, Madison, WI 53706-1687, USA

Received 12 July 2002

Abstract

The figure of merit for structural damping and damping layer applications is the product of stiffness E and damping $\tan \delta$. For most materials, even practical polymer damping layers, $E \tan \delta$ is less than 0.6 GPa. We consider several methods to achieve high values of this figure of merit: high damping metals, metal matrix composites and composites containing constituents of negative stiffness. As for high damping metals, damping of polycrystalline zinc was determined and compared with InSn studied earlier. Damping of Zn is less dependent on frequency than that of InSn, so Zn is superior at high frequency. High damping and large stiffness anomalies are possible in viscoelastic composites with inclusions of negative stiffness. Negative stiffness entails a reversal of the usual directional relationship between force and displacement in deformed objects. An isolated object with negative stiffness is unstable, but an inclusion embedded in a composite matrix can be stabilized under some circumstances. Ferroelastic domains in the vicinity of a phase transition can exhibit a region of negative stiffness. Metal matrix composites containing vanadium dioxide were prepared and studied. The concentration of embedded particles was sensitive to the processing method.

© 2003 Elsevier B.V. All rights reserved.

Keywords: Viscoelasticity; Anelasticity; Internal friction; Composites

1. Introduction

High damping materials are used to reduce vibration in aircraft, automobiles and other machinery. Reduced vibration can lead to reductions in fatigue and failure of structural parts, improved efficacy of the airplane pilot or car driver due to reduced noise, and improved passenger comfort and satisfaction. Similarly in machinery, noise reductions benefit the user. The *figure of merit* for free damping layers is proportional to $E \tan \delta$ for the layer. In many applications, bending is important, so Young's modulus E is considered as a measure of stiffness. Here, δ is the phase angle between stress and strain. It is called the *loss angle*. The loss tangent $\tan \delta$ is also the ratio E''/E' , with E'' as the loss modulus, the component of stiffness out of phase with the driving force. E' is the component of stiffness in phase with the driving force. Some authors refer to the *quality factor* Q which represents how sharp and intense a resonance peak is. If the damping is not too large, the relationship is $\tan \delta = 1/Q$. In viscoelastic

materials it is possible to achieve high stiffness and low loss, or high loss and low stiffness, but materials which combine high damping and stiffness are not common, as shown in Fig. 1. The diagonal line in Fig. 1 presents the largest product ($E \tan \delta = 0.6$ GPa) of stiffness E , considered as the absolute value of the complex dynamic Young's modulus $|E^*|$, and damping, found in common materials. Polymeric layers [1] are presently used in many applications to damp vibration [2,3]. For materials of the highest damping ($\tan \delta > 1$), the full-width at half-maximum of the damping peak at constant frequency may be only about 18 °C. Moreover available polymer damping layers have a figure of merit $E \tan \delta$ less than 0.6 GPa. It is therefore desirable to study alternate materials for damping applications.

In view of the limitations of polymer damping materials, metals [4] and their composites have been considered. For example manganese-copper (Mn-Cu) alloys, given the trade name 'Sonoston', are used for ship propellers used in naval applications. Mn-Cu alloys are non-linear: their damping performance depends on strain level. They offer little damping at small strain; moreover their behavior is temperature dependent [5]. Substantial viscoelastic response in metals may be associated with a high homologous temperature

* Corresponding author. Tel.: +1-608-265-8697;

fax: +1-608-263-7451.

E-mail address: lakes@engr.wisc.edu (R.S. Lakes).

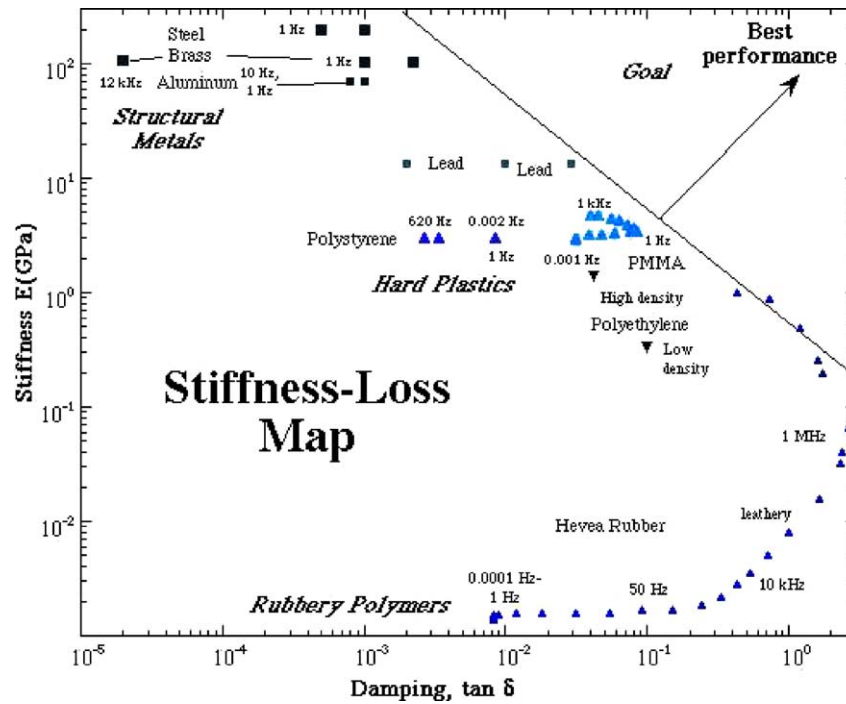


Fig. 1. Stiffness loss map, showing experimental results for Young's modulus E and mechanical damping $\tan \delta$ for various common materials at selected frequencies at room temperature (20°C). The diagonal line represents the figure of merit $|E^*| \tan \delta = 0.6 \text{ GPa} = \text{constant}$. Most common materials including polymer damping layers, occupy regions to the left of that line. Adapted from Lakes [37].

$T_H > 0.5$ in which $T_H = T/T_{\text{melting}}$, with T as the absolute temperature [6]. Some low melting point metals [7,8] such as lead and tin exhibit relatively high damping compared with structural metals but are unremarkable for the figure of merit $E \tan \delta$. Eutectic In–Sn alloy, which exhibits substantial damping $\tan \delta$ exceeding 0.1 at sub-audio frequency and a shear modulus of $G = 7.5 \text{ GPa}$, and a Young's modulus $E = 21 \text{ GPa}$, has been previously studied in depth [9]. Pure zinc is of some interest as a damping material since it is fairly stiff (a Young's modulus of 100 GPa compared with 70 GPa for aluminum and 200 GPa for steel); cast zinc has moderate damping: the loss tangent is about $\tan \delta = 0.01$ over a range of frequency. Zinc alloys such as zinc–aluminum alloy ZA27 studied by Ritchie et al. [10], has a small $\tan \delta = 0.001$ above 1 kHz. In view of the large thermal expansion of zinc, a thermoelastic damping peak of magnitude approaching 0.01 may be observed in flexure. Since this damping depends on heat flow, the frequency of the peak depends on the thickness of the specimen or metal part. The specimens studied by Ritchie et al. were about 1.2 mm in thickness which gave rise to a thermoelastic peak near 40 Hz.

Metal matrix composites have been used to achieve enhanced properties such as high specific modulus, strength, and thermal stability. Even so, composite design with consideration of viscoelastic properties, even creep, of particulate reinforced metal matrix composites, is not common [11]. In viscoelastic composites, the best viscoelastic response (highest figure of merit $E \tan \delta$) is achieved by incorporating inclusions of the maximum possible stiffness into a compliant, high damping matrix [12]. By contrast, soft high

damping inclusions in a stiff matrix give rise to low damping for given stiffness. Stiff particle inclusions are superior to fibers in this context, even though they provide less stiffening effect for a given volume fraction. Composite materials based on a metal (eutectic InSn) matrix and bonded tungsten laminae exhibited a high figure of merit $E \tan \delta$ at low frequency [12]. These constitute a proof of concept; since they contain tungsten, which is both dense and expensive, their applicability would be limited. As for alternate constituent phases, SiC has a high stiffness, $E = 430 \text{ GPa}$, low density, $\rho = 3.2 \text{ g/cm}^3$, and reasonable cost. It has been used with InSn to make high damping composites [13], but it is more difficult to achieve the required high inclusion concentration with particles than with laminae.

A different conceptual scheme for high damping composites involves inclusions of negative stiffness. Composite materials based on ferroelastic inclusions [14] which have negative stiffness [15] in the vicinity of a phase transformation, provide large peaks in mechanical damping over a range of temperature. Ordinarily, negative stiffness entails instability, but inclusions of negative stiffness can be stabilized [16] in a composite by the surrounding matrix. Vanadium dioxide is a ferroelastic material [17,18]. It undergoes a transformation from monoclinic to tetragonal at $T_c = 67^\circ\text{C}$. Negative stiffness in the vicinity of phase transformations is inferred from the fact that the energy versus deformation diagram [19] exhibits at least two relative minima or energy wells. Composites with negative stiffness inclusions are of particular interest because they permit one to exceed accepted bounds on properties. Bounds [20]

on properties of composite materials are generally derived assuming positive phase properties. These bounds can be exceeded if negative stiffness is allowed. The causal mechanism for the damping maximum and variation in stiffness in the vicinity of the transition is a greater deformation in and near the inclusions than in the composite as a whole. This can allow extreme properties not previously anticipated.

Negative stiffness can be visualized as follows. Macroscopic lumped examples of negative stiffness include a column constrained in a buckled 'S' shaped configuration [21]. If one presses laterally on the column, one can cause it to snap through. The negative stiffness condition is unstable. The column can be stabilized by a lateral constraint. That constraint may contain a spring element of positive stiffness. Negative stiffness is to be distinguished from negative Poisson's ratio [22]. Poisson's ratio is the ratio of lateral contraction strain of a stretched object divided to its longitudinal strain. Flexible tubes after compressive buckling exhibit decreasing force with an increase in deformation, hence they have negative incremental stiffness. Single cell tetrakaidecahedron models of polymer foam cells exhibit a non-monotonic compressive force-deformation relation [23] under displacement control. These therefore exhibit negative stiffness over a range of strain. Macroscopic elements of positive and negative stiffness in series give rise to mechanical damping orders of magnitude greater than that of the constituent material, provided the positive and negative stiffness is balanced by tuning the prestrain, which governs the degree of instability in the negative stiffness elements [24].

In the present work, damping and stiffness of pure zinc (as a potential composite constituent) and of Sn-VO₂ composites are studied at acoustic frequencies.

2. Materials and methods

2.1. Metal preparation

Metals were cast as follows. A hydraulic press (Carver) and heating apparatus was used to press pieces from a zinc ingot (>99.99%, Alfa Aesar, Ward Hill, MA) to approximately 20,000 lbs for 2–10 min. This resulted in thin sheets of metal which were cut into small pieces. These pieces were inserted into a Pyrex glass tube 3 mm in inside diameter with one end sealed shut with a torch. A steel rod was placed in the upper end to aid in consolidation. The sample tube was then placed in a 7 mm inner diameter Pyrex tube capped to reduce oxidation. The furnace was preheated to 480 °C. When the melting had begun the sample was tamped by dropping the tube vertically onto a foil-covered piece of foam to assist in consolidation. Once the sample was completely melted and consolidated the furnace door was opened to abruptly cool the chamber to 420 °C. Final cooling was done within the furnace for slow cooling. More rapid cooling was done by removing the specimen tube into room air

and exposing it to air flow from a fan. The glass tube was then cracked by compression and the sample removed and cut with a diamond saw to about 3 cm length.

2.2. Composite preparation

Composite materials were prepared with inclusions of vanadium dioxide (VO₂) in a pure (99.99%) tin matrix. Particulate inclusions of 150 μm size or smaller were incorporated into a tin matrix by rolling sheets of tin with particles, followed by casting into a cylindrical mold 3 mm in diameter. Specifics are as follows: a block of tin (Alfa Aesar, Ward Hill, MA) was rolled into a thin square sheet using a commercial powered roller (Stanat MFG Co., Model No. TA-315, Westbury, NY). A tin sheet with an area of at least 26 cm² and a thickness of about 0.8 mm was produced in the rolling process. Once the tin was flattened, the surface was cleaned with acetone to remove oxidation and grease from the rollers. A layer of fine vanadium dioxide particles (about 5% of the total target amount of VO₂ by weight) was sprinkled on the tin sheet, which was then folded by hand and rolled again to obtain the desired thickness. Reduction in thickness by a factor of two was necessary to achieve adhesion. Every third or fourth layer, no vanadium dioxide particles were embedded to facilitate the compaction of the previous layers. Cracked edges were trimmed with a razor and their weights measured using a scale. Total weight of trimmed tin matrix was subtracted from the original tin weight to determine the final concentration of particles. Folding directions were consistently alternated by 90° to achieve straighter edges. At least 40 passes through the rollers were conducted to achieve the desired concentration of particles with a uniform distribution. A portion of the tin sheet was rolled tightly into a glass cylindrical tube of inner diameter 3 mm inclined at 45° from the horizontal and melted in a furnace. The melting was done quickly and the tube removed from the furnace to cool while being slowly rotated about its axis, in the air.

2.3. Test methods

Optical micrographs of specimens were obtained using an Olympus (Melville, NY) type BH2-1 microscope with a digital camera (Diagnostic Measurements, model 3.2.0, Sterling Heights, MI) and image capture system. Each specimen was cut with a low speed diamond saw and was ground and polished with graded metallographic abrasives prior to microscopic observation.

Viscoelastic testing on the samples was performed by using the broadband viscoelastic spectroscopy (BVS) apparatus [25,26], as shown in Fig. 2. The apparatus is capable of measuring mechanical properties of materials in a 11 decade frequency range, from 10⁻⁶ up to 10⁵ Hz without appeal to time-temperature superposition, assumptions of Arrhenius temperature dependence of properties, or any other temperature related calculations. The rationale is to enable study of

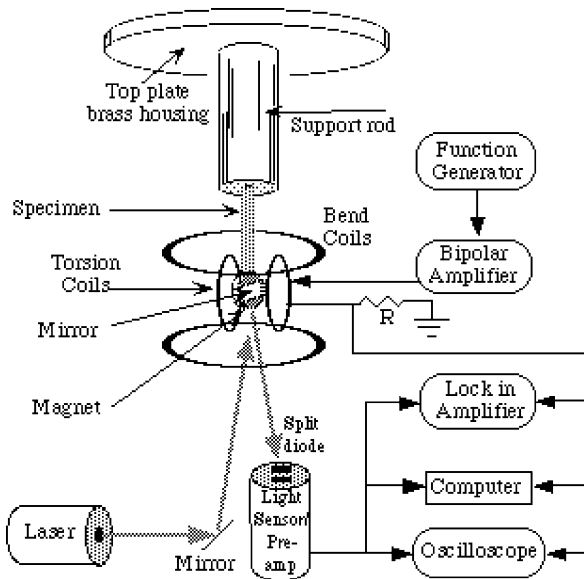


Fig. 2. Schematic diagram of the broadband viscoelastic spectroscopy apparatus. For high frequency studies, the driving magnet may be cubical, the same thickness as the specimen.

heterogeneous specimens including composites, for which such inferences are not justified. The wide frequency range is achieved by choosing a specimen geometry amenable to a simple analytical solution so that data can be readily interpreted, and by using drive and detection methods free of resonances and low-frequency cut-offs.

Specimens were mounted on a support rod by cyanoacrylate cement. A permanent magnet and mirror were cemented on the free end of the specimen to provide torque and measurement of angular displacement. The cement between interfaces was allowed to cure for 24 h. For high stiffness specimens, a tungsten support rod, which has a Young's modulus twice that of steel, was adopted. Also, the instrument was modified by providing the ability to use a 25.4 mm (1 in.) diameter stainless steel support rod. This has 16 times the torsional rigidity of a 12.7 mm (0.5 in.) diameter steel rod. These modifications reduce the parasitic compliance and damping for stiff specimens.

Torque was generated by the interaction between the permanent magnet and the Helmholtz coil inside the apparatus. For torsion, the electrical signal was input in the torsion coil, which is oriented so the torque on the permanent magnet (the cross product of applied magnetic field and the magnet's magnetic moment) is in the correct direction. For bending, the signal was input to a bending coil oriented perpendicularly as shown in Fig. 2. The sensitivity direction of the angular displacement measurement was rotated by 90° by inserting a dove prism into the laser beam path. The frequency of the torque was controlled by the frequency of electrical currents from a function generator to the coil. For stiff, stubby specimens, the mirror was mounted on the sample, not on the magnet, to eliminate errors from the compliance of the cement. The sample and coil were put inside

a massive brass chamber supported by a vibration isolator. A mirror reflected the diode laser beam from the specimen end mirror to a split-diode light detector. The light detector converted the spatial movement of the laser beam into an electrical signal, and the signal was captured by an oscilloscope and computer. The use of a lock-in amplifier (Stanford Research Systems, SR850) facilitated measurement of the loss tangent with high accuracy. In addition, the method of determining the width of digitized Lissajous curves was also adopted to verify the experimental data. Data reduction was achieved by following previous well-developed procedures for ultra low, sub-resonant, and resonant frequency ranges. The electrical input was sinusoidal for dynamic studies and a step function for creep studies.

Data reduction of torsion experiments may be done using an exact relationship [27] for the torsional rigidity (ratio of torque M^* , including its phase, to angular displacement ϕ) of a viscoelastic cylinder of radius R , length L , and density ρ fixed at one end with a mass of mass moment of inertia I_{at} at the other end:

$$\frac{M^*}{\phi} = \frac{1}{2} \rho \pi R^4 \omega^2 L \frac{\cot \Omega^*}{\Omega^*} - I_{at} \omega^2 \quad (1)$$

where $\Omega^* = (\rho \omega^2 L^2 / G^*)^{1/2}$ with G^* as the complex shear modulus which has a phase angle δ , ν as frequency and $\omega = 2\pi\nu$. Below the first natural frequency, it was sufficient to use the following equations for calculating the modulus and loss tangent. The observed phase angle is φ the structural phase angle.

$$\tan \delta = \left[1 - \left(\frac{\nu}{\nu_0} \right)^2 \right] \tan \varphi \quad (2)$$

This expression corrects for the effect of the fundamental resonance. At low frequency the shear modulus was obtained from:

$$G^* = \frac{2M^*L}{\phi\pi R^4} \quad (3)$$

At resonance frequencies ν_0 , $\tan \delta$ was obtained from the width $\Delta\nu = \nu - \nu_1$ of the resonance curve (the plot of dynamic compliance ϕ/M versus frequency) at half the maximum amplitude.

$$\tan \delta \approx \frac{\Delta\nu}{\nu_0\sqrt{3}} \quad (4)$$

For quasistatic bending, at low frequency, Young's modulus was obtained from:

$$E^* = \frac{4M^*L}{\phi\pi R^4} \quad (5)$$

Temperature dependence of properties was studied as follows. The specimen was driven at a constant frequency (100 Hz) well below the lowest natural frequency. An insulated inner chamber was heated to above 85 °C and maintained for at least 30 min. The heater was shut-off and the chamber allowed to cool. Cooling rate over the temperature

range of interest was less than 1 K/min. A lock-in amplifier was used to take repeated measurements at the selected frequency during the cooling process.

3. Results and discussion

3.1. Zinc

Optical microscopic analysis of the structure of zinc specimens showed that furnace cooling gave rise to large crystals on the order of a millimeter in size. Rapid cooling gave rise

to a smaller grain size, but the crystals are still fairly large: several hundred microns. The frequency dependence of the properties of furnace cooled and rapidly cooled Zn is shown in Fig. 3. The damping of zinc varies little with frequency, in contrast to InSn in which $\tan \delta \propto \nu^{-n}$ over many decades where ν is frequency and $n = 0.28$ for eutectic InSn, and $n = 0.22$ for γ -InSn. For other metals at high homologous temperature, n has a value in the range $0.1 \leq n \leq 0.5$. For example $n = 0.10$ for SnCd, 0.12 for SnSb [28] and 0.44 for InSnCd [29] at room temperature. The polycrystalline zinc studied here has considerably higher mechanical damping than zinc single crystals [30,31] for which $\tan \delta$ can be

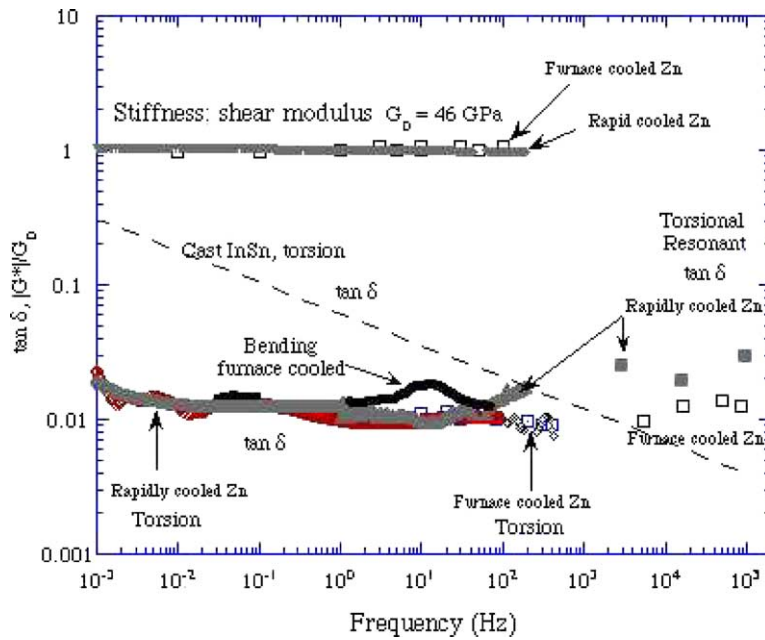


Fig. 3. Frequency dependence of torsional viscoelastic properties of cast pure Zn, rapidly cooled (solid gray symbols) compared with furnace cooled (open symbols). Damping in bending exhibits a peak attributed to thermoelastic coupling. Shown for comparison is the behavior of eutectic InSn (dash line) [9].

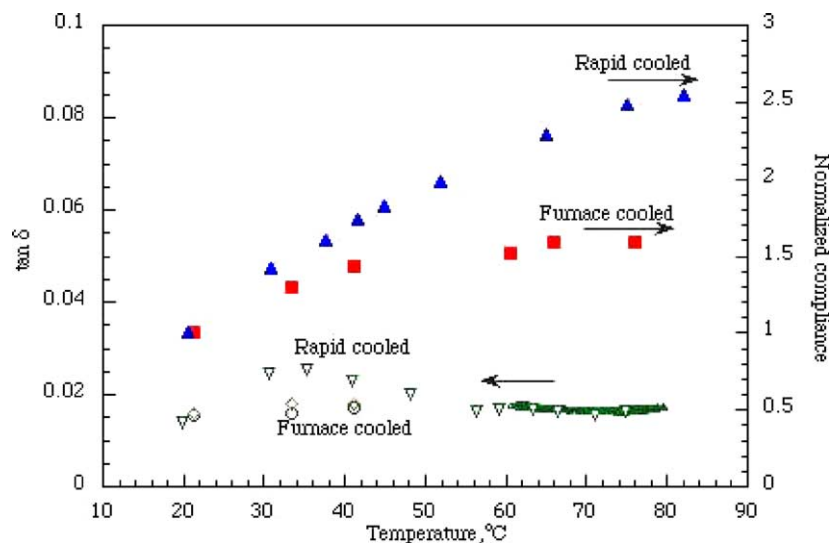


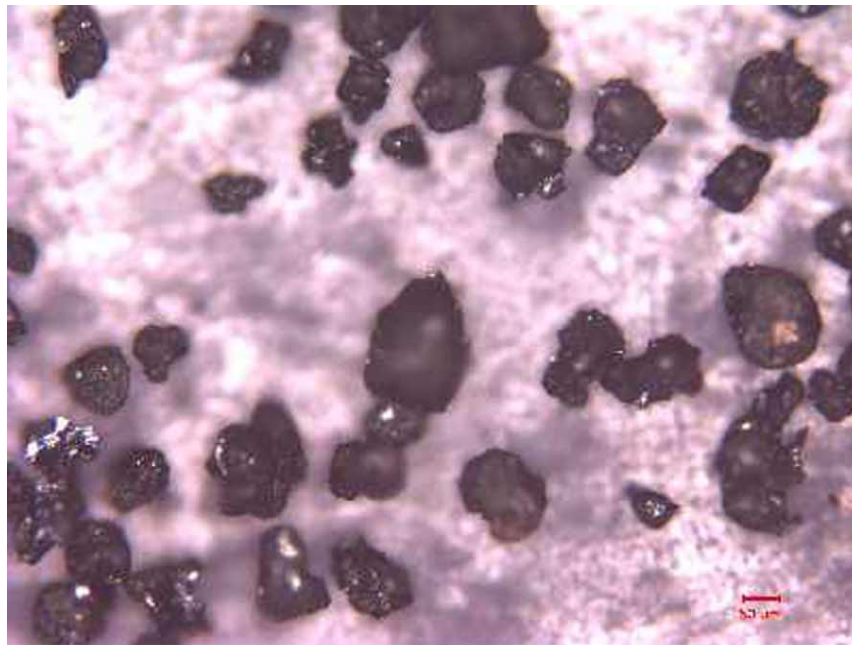
Fig. 4. Temperature dependence of torsional viscoelastic properties of cast pure Zn, rapidly cooled compared with furnace cooled at 100 Hz.

less than 10^{-5} (at 39 kHz). The difference in damping is attributed to dislocations associated with boundaries. Viscous sliding of grain boundaries, which usually gives rise to a well-defined peak, cannot be responsible for the broadband damping observed.

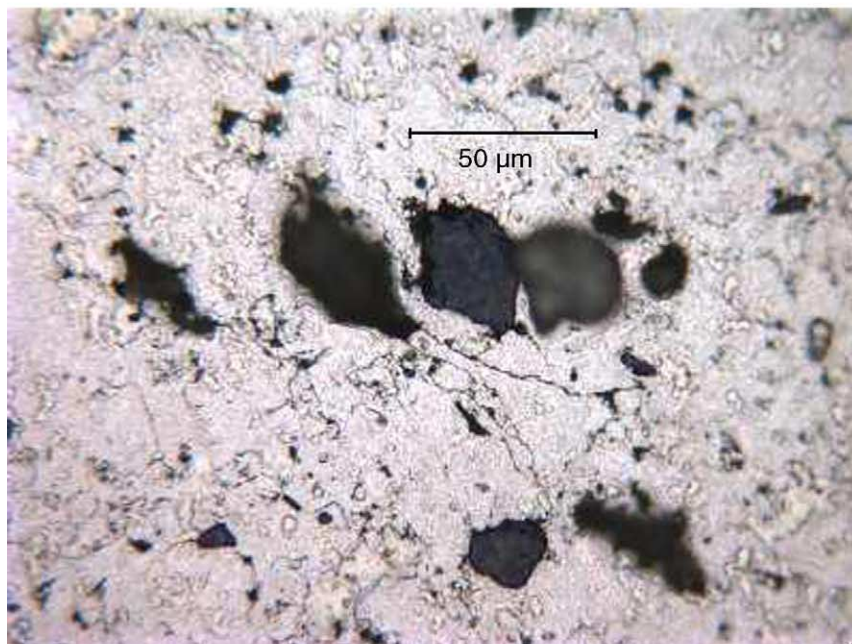
The difference between the two different processed samples is not significant at low frequency, however the rapidly cooled sample shows an increase of $\tan \delta$ at high frequency.

This might be due to additional dislocations formed during the process. Temperature dependence at 100 Hz of the two different processed Zn samples shows significantly different viscoelastic properties (Fig. 4). The compliance is normalized to that at 1 Hz at room temperature. Rapidly cooled Zn is more temperature dependent than furnace cooled Zn.

The causal mechanisms for metal damping are considered to be based on the paradigm of dislocation based damping.

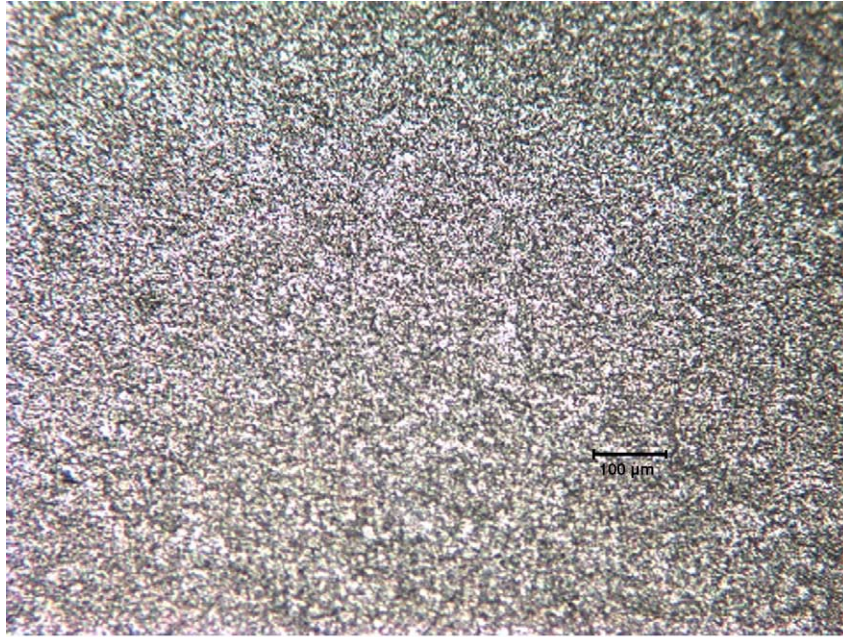


(a)



(b)

Fig. 5. Optical micrographs of Sn-VO₂ composite. (a) VO₂ particles: 50 μm scale bar; (b) Sn-VO₂ composite, rapid cooling: 50 μm scale bar; (c) Sn-VO₂ composite, slow cooling: 100 μm scale bar.



(c)

Fig. 5. (Continued).

To place that in context, an early model for the high temperature background is the dislocation-point defect damping of Schoeck et al. [32]. At sufficiently high frequency ν , $\tan \delta \propto \nu^{-1}$, a dependence on frequency which is not observed. For a distribution of activation energies, Schoeck et al. obtained, for the case of zero restoring force on the dislocations, $\tan \delta \propto \nu^{-n}$. They could not calculate the value of n but suggested $n < 1$. Cagnoli et al. [33] suggested that such a model cannot account for damping at low frequency. Cagnoli et al., assuming self-organized criticality of stick-slip dislocation processes calculated $\tan \delta \propto \nu^{-2}$. That theory cannot account for the behavior of Zn or InSn or other metals referred to earlier. A more recent dislocation based theory [34] gives $\tan \delta \propto (-\ln \nu)^3$. This would be satisfactory for the low-melting point metals such as InSn, SnCd and others over a relatively narrow frequency window, but it fails to model the behavior over 11 decades. The relatively flat frequency response of Zn observed in the present results cannot be accommodated by such a theory. It is not yet possible to predict the slope n for any material or to explain why different materials exhibit different values of n .

Thermoelastic effects [35,36] can contribute to the damping of bent bars, in which the strain field is heterogeneous. Since the effect depends on thermal expansion, the strain field must contain a volumetric component. Thermoelastic damping due to stress-induced heat flow in a circular cylindrical rod vibrating in bending has a characteristic frequency ν_0 :

$$\nu_0 = 0.539 \frac{k}{C_v} \frac{1}{r^2} \quad (6)$$

with r as radius, k as the thermal conductivity and C_v as the heat capacity per unit volume. For zinc, $k = 113 \text{ J}/(\text{s m K})$,

$C_v = 383 \text{ J}/(\text{kg K})$. The density, $\rho = 7.13 \times 10^3 \text{ kg}/\text{m}^3$ is used in the calculation to convert the heat capacity to a mass basis. So, for a rod 3.3 mm in diameter (corresponding to the size of the specimen), $\nu_0 = 8.2 \text{ Hz}$. The relaxation strength for this kind of damping is given by

$$\Delta = \frac{E\alpha^2 T}{c\rho} \quad (7)$$

with E as Young's modulus, α as thermal expansion coefficient, ρ as density, c as heat capacity per unit mass, and T as absolute temperature. For zinc, $\Delta = 0.018$, so for a Debye peak the maximum $\tan \delta = 0.009$. This is the strongest thermoelastic damping among common materials. In the present results for zinc, the elevation of damping observed in the bending of zinc in comparison with torsion near 10 Hz is attributed to thermoelastic coupling.

3.2. Composites

High damping composite materials can be achieved in at least two ways. First, one can combine a stiff, low damping phase with a more compliant high damping phase using an optimal inclusion morphology. As an illustration of that approach, SiC–InSn composites were fabricated and tested [12] as discussed above. Since InSn has high loss with moderate stiffness ($E = 21 \text{ GPa}$; $G = 7.5 \text{ GPa}$), it was chosen as a matrix material for composites with SiC. Second, one can make use of inclusions of negative stiffness. Vanadium dioxide was chosen as the inclusion material since it undergoes a phase transition near 67°C . This phase transition gives rise to negative stiffness in the vicinity of the transition. Optical micrographs of inclusions and of Sn–VO₂ composite are shown in Fig. 5. Fig. 5(a) shows

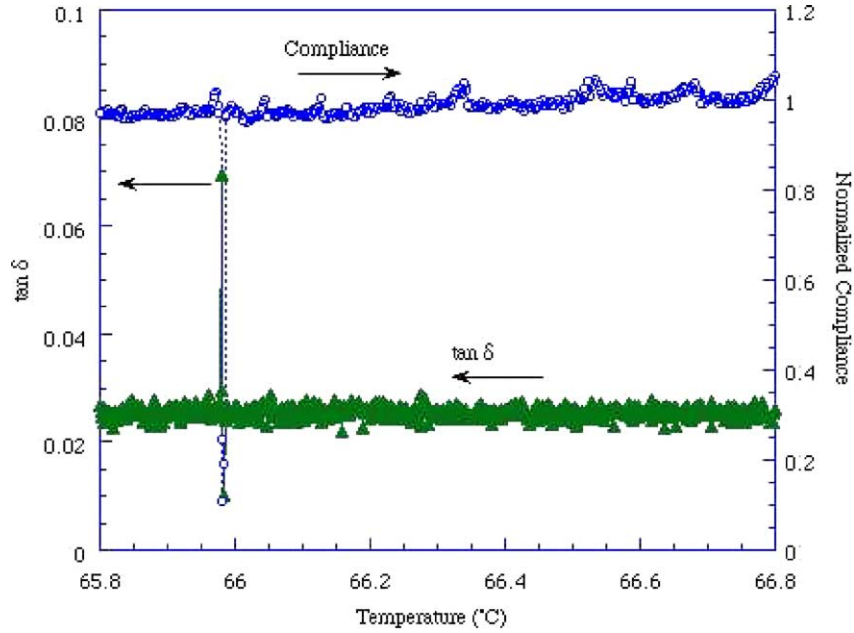


Fig. 6. Experimental torsional compliance and mechanical damping $\tan \delta$ vs. temperature for ferroelastic composite. Filled triangles, a composite containing 1% (v/v) vanadium dioxide particles in a tin matrix. Points, pure tin for which $\tan \delta = 0.019$ over the temperature range considered. Measurements were conducted at 100 Hz, well below resonance, during slow cooling through the ferroelastic transition of the inclusions.

inclusions prior to incorporation in a composite. Processing technique proved to be crucial in successfully making these composites. Rapid heating and cooling led to a distribution of particles as shown in Fig. 5(b). Volume concentration of particles estimated from a set of such images was on the order 1%, corresponding to the intended concentration.

The particles were fragmented into smaller pieces, some less than 10 μm , by the rolling process. The effects sought in these composites depend on single domain inclusions. Therefore, this fragmentation can be beneficial. The domain size of VO_2 is not available. For specimens held too long (10 min) above the matrix melting point, the particles

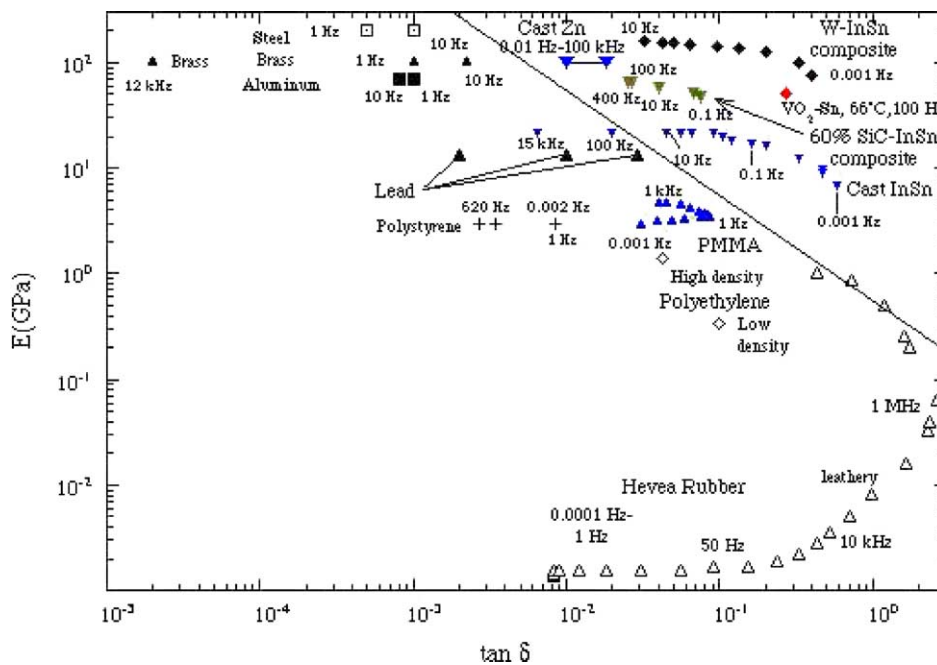


Fig. 7. Stiffness loss map, showing experimental results for Young's modulus E and mechanical damping $\tan \delta$ for materials examined in the present study and in [9,12,14]. Cast zinc is superior to InSn at the higher frequencies. All values are at room temperature except for those for Sn- VO_2 composite, which are for 66°C.

segregated and did not appear in the cross section, as shown in Fig. 5(c). Therefore, rapid processing is essential to the production of low-concentration composites by this method.

Stiffness and damping versus temperature of a particulate Sn–VO₂ composite with 1% (v/v) of inclusions exhibited sharp variations not seen in the pure Sn matrix [14]. In some cases, a large excursion in dynamic compliance was observed, as shown in Fig. 6. A stiffness loss map summarizing the performance of metals and composites is shown in Fig. 7. Zinc is superior to InSn at the higher frequencies since its damping does not vary much with frequency in comparison with InSn. The Sn–VO₂ composite requires sharp tuning of temperature to achieve extreme properties. For practical damping composites, the tuning range would have to be broadened. That is a topic for further study.

4. Conclusions

- (i) The mechanical damping of zinc exhibits little dependence on frequency over a wide range. At high frequency it has a higher damping than InSn and other high damping metals.
- (ii) Composites with inclusions of negative stiffness based on ferroelastic inclusions achieve high damping via temperature tuning.
- (iii) Composites with inclusions of negative stiffness require relatively rapid cooling of the melt to prevent segregation of the inclusion particles. Rolling of layers prior to casting results in fragmentation of the inclusions.

Acknowledgements

The authors are grateful for a grant, CMS-9896284, from NSF and for the NSF-REU program. We thank B. Welbes and C. Marquez for assistance in preparing specimens and W. Drugan and R. Cooper for helpful comments and discussion.

References

- [1] R.N. Capps, L.L. Beumel, in: R.D. Corsaro, L.H. Sperling (Eds.), *Sound and Vibration Damping with Polymers*, American Chemical Society, Washington, DC, 1990.

- [2] L. Cremer, M. Heckl, *Structure Borne Sound*, second ed., Springer, Berlin, 1987.
- [3] A.D. Nashif, D. Jones, J.P. Henderson, *Vibration Damping*, Wiley, NY, 1985.
- [4] D.W. James, *Mater. Sci. Eng.* 4 (1969) 1/8.
- [5] E.J. Graesser, C. Wong, DTRC-SME-91/34, David Taylor Research Center, Bethesda, MD, July 1991.
- [6] J. Quackenbush, M. Brodt, R.S. Lakes, *Scripta Metall.* 35 (1996) 441–447.
- [7] R. Kamel, *Phys. Rev.* 75 (1949) 1606.
- [8] L.S. Cook, R.S. Lakes, *Scripta Metall. Mater.* 32 (1995) 773–777.
- [9] R.S. Lakes, J. Quackenbush, *Philos. Magaz. Lett.* 74 (1996) 227–232.
- [10] I.G. Ritchie, Z.L. Pan, F.E. Goodwin, *Met. Trans.* 22A (1991) 617–622.
- [11] I.A. Ibrahim, F.A. Mohamed, E.J. Lavernia, *J. Mater. Sci.* 26 (1991) 1137–1156.
- [12] M. Brodt, R.S. Lakes, *J. Comp. Mater.* 29 (1995) 1823–1833.
- [13] M. Ludwigson, C.C. Swan, R.S. Lakes, *J. Comp. Mater.* 36 (2002) 2245.
- [14] R.S. Lakes, T. Lee, A. Bersie, Y.C. Wang, *Nature* 410 (2001) 565–567.
- [15] R.S. Lakes, *Phys. Rev. Lett.* 86 (2001) 2897–2900.
- [16] R.S. Lakes, W.J. Drugan, *J. Mech. Phys. Solids* 50 (2002) 979–1009.
- [17] R. Heckingbottom, J.W. Linnett, *Nature* 194 (1962) 678.
- [18] D. Paquet, P. Leroux-Hagon, *Phys. Rev. B* 22 (1979) 5284–5301.
- [19] E. Salje, *Phase Transitions in Ferroelastic and Co-elastic Crystals*, Cambridge University Press, Cambridge, 1990.
- [20] Z. Hashin, S.A. Shtrikman, *J. Mech. Phys. Solids* 11 (1963) 127–140.
- [21] Z. Bazant, L. Cedolin, *Stability of Structures*, Oxford University Press, Oxford, 1991.
- [22] R.S. Lakes, *Science* 235 (1987) 1038–1040.
- [23] P. Rosakis, A. Ruina, R.S. Lakes, *J. Mater. Sci.* 28 (1993) 4667–4672.
- [24] R.S. Lakes, *Philos. Magaz. Lett.* 81 (2001) 95–100.
- [25] C.P. Chen, R.S. Lakes, *J. Rheol.* 33 (8) (1989) 1231–1249.
- [26] M. Brodt, L.S. Cook, R.S. Lakes, *Rev. Sci. Instrum.* 66 (1995) 5292–5297.
- [27] W.G. Gottenberg, R.M. Christensen, *Int. J. Eng. Sci.* 2 (1964) 45–56.
- [28] J. Quackenbush, M. Brodt, R.S. Lakes, *Scripta Metall. Mater.* 35 (1996) 441–447.
- [29] M. Brodt, R.S. Lakes, *J. Mater. Sci.* 31 (1996) 6577–6581.
- [30] T.A. Read, *Phys. Rev.* 58 (1940) 371–380.
- [31] J. Weertman, *J. Appl. Phys.* 26 (1955) 202–210.
- [32] G. Schoeck, E. Bisogni, J. Shyne, *Acta Metall.* 12 (1964) 1466–1468.
- [33] G. Cagnoli, L. Gammaitoni, F. Marchesoni, D. Segoloni, *Philos. Magaz. A* 68 (1993) 865–870.
- [34] G. D’Anna, W. Benoit, V.M. Vinokur, *J. Appl. Phys.* 82 (1997) 5983–5990.
- [35] C. Zener, *Phys. Rev.* 52 (1937) 230–235.
- [36] C. Zener, *Phys. Rev.* 53 (1938) 90–99.
- [37] R.S. Lakes, *Viscoelastic Solids*, CRC Press, Boca Raton, FL, 1998.